Processing and Low Voltage Switching of Organic Ferroelectric Phase-Separated Bistable Diodes

Li, Mengyuan; Stingelin, Natalie; Michels, Jasper J.; Spijkman, Mark-Jan; Asadi, Kamal; Beerends, Rene; Biscarini, Fabio; Blom, Paul W. M.; de Leeuw, Dago M.

Published in:
Advanced Functional Materials

DOI:
10.1002/adfm.201102898

ADVANCED FUNCTIONAL MATERIALS
www.afm-journal.de

Processing and Low Voltage Switching of Organic Ferroelectric Phase-Separated Bistable Diodes

Mengyuan Li, Natalie Stingelin, Jasper J. Michels, Mark-Jan Spijkman, Kamal Asadi, Rene Beerends, Fabio Biscarini, Paul W. M. Blom, and Dago M. de Leeuw**

The processing of solution-based binary blends of the ferroelectric random copolymer poly(vinylidene fluoride-trifluoroethylene) P(VDF-TrFE) and the semiconducting polymer poly(9,9-dioctylfluorenyl-2,7-diyl) (PFO) applied by spin-coating and wire-bar coating is investigated. By systematic variation of blend composition, solvent, and deposition temperature it is shown that much smoother blend films can be obtained than reported thus far. At a low PFO:P(VDF-TrFE) ratio the blend film consists of disk-shaped PFO domains embedded in a P(VDF-TrFE) matrix, while an inverted structure is obtained in case the P(VDF-TrFE) is the minority component. The microstructure of the phase separated blend films is self-affine. From this observation and from the domain size distribution it is concluded that the phase separation occurs via spinodal decomposition, irrespectively of blend ratio. This is explained by the strong incompatibility of the two polymers expressed by the binary phase diagram, as constructed from thermal analysis data. Time resolved numerical simulation of the microstructure evolution during de-mixing qualitatively shows how an elevated deposition temperature has a smoothening effect as a result of the reduction of the repulsion between the blend components. The small roughness allowed the realization of bistable rectifying diodes that switch at low voltages with a yield of 100%. This indicates that memory characteristics can be tailored from the outset while processing parameters can be adjusted according to the phase behavior of the active components.

1. Introduction

Organic electronics has emerged as a promising technology for large-area microelectronic applications such as rollable displays,[1] electronic paper,[2] contactless identification transponders,[3,4] and smart labels.[5] Most of these applications require memory functions, preferably based on a non-volatile memory that i) retains its data when the power is turned off and ii) can be programmed, erased, and non-destructively read-out by electrical pulses. In the ultimate memory the discrete elements are integrated into a cross-bar array, i.e., an unpatterned storage medium that is sandwiched between rows and columns of metal electrode lines where each intersection makes up one memory bit.[6] By using an un-patterned storage medium the array is simple to make because it does not require strict alignment.

Realization of true cross-bar arrays is hampered when using electrically symmetric switching elements. The reason is that the performance of such arrays is limited by cross talk between the individual devices, meaning that the measured resistance equals that of the selected cell in parallel with the resistances of the memory cells in all other word and bit lines. Reliable determination of the logic value, thus, requires electrical isolation of the discrete cells. The isolation can be realized by using one blocking electrode.[7] In such a geometry, each intersection acts as a rectifying bistable diode. Recently, 9-bit cross-talk free memory arrays in a $4F^2$ cell configuration (where F is the width of the electrode lines and spacings) have

M. Li, Dr. M. Spijkman, Prof. P. W. M. Blom, Prof. D. M. de Leeuw
Zernike Institute for Advanced Materials
University of Groningen
Nijenborgh 4, 9747 AG, Groningen
The Netherlands
E-mail: mengyuan.li@rug.nl; dago.de.leeuw@philips.com
Dr. N. Stingelin
Department of Materials and Centre for Plastic Electronics
Imperial College London
Exhibition Road, London, SW7 2AZ, UK
Dr. N. Stingelin
FRIAS, School of Soft Matter Research
University of Freiburg
79104 Freiburg, Germany
Dr. J. J. Michels, Prof. P. W. M. Blom
Holst Centre, High Tech Campus 31
5605 KN Eindhoven, The Netherlands
Dr. K. Asadi, R. Beerends, Prof. D. M. de Leeuw
Philips Research Laboratories
High Tech Campus 4, 5656AE, Eindhoven
The Netherlands
Prof. F. Biscarini
CNR- ISMN, Institute for the Study of Nanostructured Materials
Via Gobetti 101, I-40129 Bologna, Italy

DOI: 10.1002/adfm.201102898

been demonstrated based on such a principle, which resulted in a logic table composed of 512 different states.[8] The active layer consists of semiconducting domains, bicontinuous from top to bottom of the film, embedded in a ferroelectric matrix.[9] The polarization field of the ferroelectric component modulates the injection barrier at the semiconductor/metal contact, yielding a space charge limited on-state and an injection limited off-state.[10] Hence, the diodes can be switched at biases larger than the coercive field and the resistance can be read-out non-destructively at low bias. The switching mechanism of the ferroelectric-driven organic resistive switches is the stray field of the polarized ferroelectric phase.[11] A review of non-volatile ferroelectric blend diodes has been published.[12] Undesirably, though, the phase-separated nature of the active layer of the semiconducting and ferroelectric component leads to a film roughness that, when spin-coated, is comparable to the layer thickness. As a consequence, evaporation of the top metal results in electrical shorts and the fabrication yield of such structures is low. Therefore, functional switches have so far only been realized with relatively thick active films of about 1 μm, which require technologically unacceptably high voltages (≈20 V) to switch the ferroelectric. This stifles the application of such switches in, for instance, contactless radio frequency identification (RFID) tags that only operate at low voltages due to the lack of wired power.

Here we demonstrate that with suitable processing smooth and thin ferroelectric/semiconducting blend films can be obtained, which allow fabrication of bistable rectifying diodes that switch below 5 V at high yield. We focus on P(VDF-TrFE):PFO binaries processed either by spin-coating or wire-bar coating using different solvents and temperatures. Their solid-state microstructure is investigated by atomic force microscopy (AFM) and X-ray diffraction (XRD). The de-mixing and solidification behavior of the blend and their dependence on processing protocol are discussed and related to the phase diagram. The time and temperature development of the topology as a result of blend phase separation has been simulated by numerical calculations. The methodology used for film fabrication, wire-bar coating, is ideally suited to deposited thin films over a large area. Hence the process developed is a major leap towards industrialization of high density non-volatile memories.

2. Spin-Coated P(VDF-TrFE):PFO Thin Films

Bistable rectifying diodes have been demonstrated with a range of binaries, including regio-irregular poly(3-hexylthiophene) (rir-P3HT),[7,9,10] phenyl-substituted poly(phenylene vinylene) commercially known as super yellow (SY),[10] and poly(9,9-dioctylfluorene) (PFO)[13] blended with poly(vinylidene fluoride-trifluoroethylene) [P(VDF-TrFE)]. Here we focus on P(VDF-TrFE):PFO, (their chemical structures are presented in **Figure 1**), for which the evolution of the phase morphology of spin-coated thin films has recently been modeled by Michels et al.[14] The model, using ternary diffuse interface theory integrated with a modified Flory–Huggins treatment of the homogeneous, bulk free energy of mixing, predicts for such blends that the phase separation occurs via spinodal decomposition. This seems to be in agreement with experimental results. The AFM phase image, presented in Figure 1a, for instance, reveals that spin-coated films of P(VDF-TrFE):PFO (90:10 weight ratio; produced following literature procedures using tetrahydrofuran (THF) as a common solvent), phase separate into circular featureless domains that are randomly embedded in the film structure. Based on previously reported scanning electron microscopy (SEM) data on P(VDF-TrFE) with rir-P3HT,[9] the circular domains can be attributed to PFO-rich domains, while the matrix is assigned to P(VDF-TrFE).[15] Such a microstructure would be desired for use in rectifying diodes. However, the roughness of the resulting films is comparable to the layer thickness (see corresponding height image in Figure 1b). As a consequence, the yield of functional capacitors and diodes fabricated with these films is unacceptably low because of the electrical shorts that are formed upon evaporation of the top electrode. This is highly unfortunate as the 90:10 blends would give optimal switching characteristics.[9] Since the binary of P(VDF-TrFE) and PFO most likely features an upper critical solution temperature (UCST)

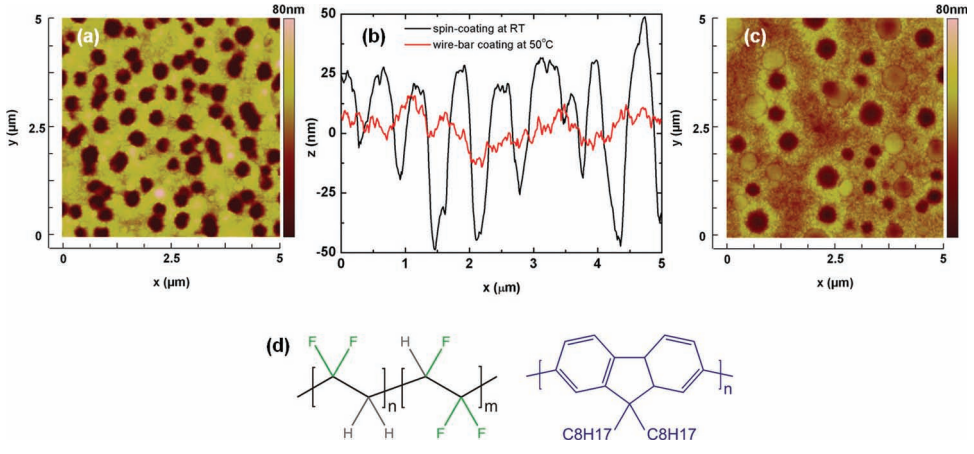

Figure 1. a) AFM phase image of a spin-coated blend film using THF as a common solvent. The P(VDF-TrFE):PFO ratio was 90:10 by weight. The image shows that the spin-coated film phase separates into circular featureless PFO domains that are randomly embedded in the P(VDF-TrFE) matrix. b) Corresponding height profile of spin-coated film form THF (black) and wire-bar coated film from cyclohexanone (red). c) AFM phase image of a wire-bar coated film at 50 °C using cyclohexanone as a common solvent. The P(VDF-TrFE):PFO ratio was 90:10 by weight. d) Chemical structure of P(VDF-TrFE) and PFO.

behavior, which means that the compatibility of these two polymers increases with temperature, we therefore set out to explore how the blend microstructure can be improved by varying the deposition temperature and by selection of solvents.

3. Wire-Bar Coated P(VDF-TrFE):PFO Thin Films

In order to control the deposition temperature accurately, we elected to produce the P(VDF-TrFE):PFO films by wire-bar coating, rather than by spin-coating.[16] To this end, films were cast at 50 °C and annealed in vacuum for 2 h at 140 °C. Reassuringly, the roughness decreased drastically upon increasing the deposition temperature (i.e., substrate temperature); in fact, **Figure 2** demonstrates that rms roughnesses below 10 nm can be realized. This is a significant improvement over spin-coated films, which featured a rms roughness of ≈100 nm, as it promises reliable fabrication of bistable diodes driven at low voltages.

4. Influence of Solvent

In addition to the compatibilization of the two components, the use of higher deposition temperatures, of course, also lead to an enhanced solvent evaporation rate. The system will vitrify at an earlier stage during deposition, which leaves, among other things, less time for solidification. We therefore attempted to disentangle these two effects and tried to elucidate if compatibilization of the two polymers at elevated temperatures or a reduced solidification rate results in smoother film morphologies. For this purpose, we selected cyclohexanone as a solvent, which has a higher boiling temperature (and thus a lower evaporation rate) than THF.

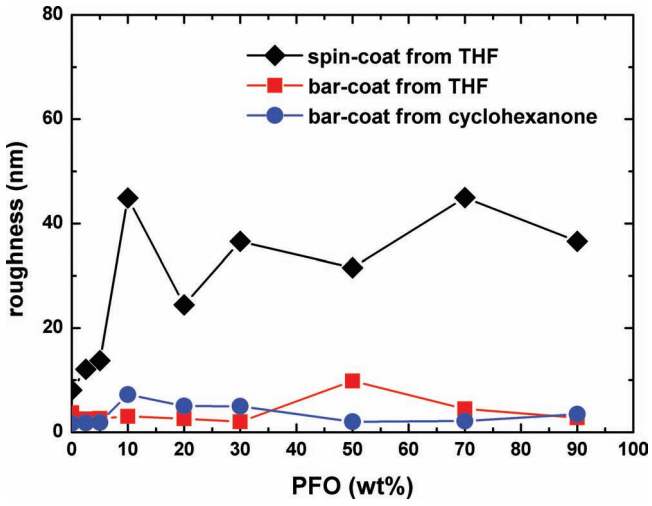

Figure 2. The rms roughness of P(VDF-TrFE):PFO blend films as a function of PFO content. The roughness was measured by AFM. Black squares are obtained from spin-coated films from THF. Red squares from wire-bar coated films from THF and red squares wire-bar coated form cyclohexanone. The substrate temperature of the wire-bar coater was 50 °C. The film thickness in all cases is about 100 nm. After deposition all films have been annealed for 2 h at 140 °C in vacuum.

The roughness of the resulting films, produced at 50 °C from cyclohexanone was again smaller than the one observed for films spin-coated from THF. This can be deduced from the AFM height profile of the 90:10 (P(VDF-TrFE):PFO) film (wire-bar coated at 50 °C) presented in Figure 1b. From plotting the roughness of blend films as a function of composition (Figure 2) the significant improvement in film quality is evident. Blend film roughness's of less than 10 nm are consistently obtained at all compositions, also when this solvent is utilized for film fabrication. Comparable results are obtained using both solvents (cyclohexanone and THF) as long as the blends are cast at elevated temperatures. This indicates that the smoothness of the resulting blend structures originates not from a vitrifying effect due to rapid solvent removal, but because the two polymers are more miscible at these temperatures.

5. Numerical Morphology Simulations

Close inspection of the AFM images reveals why selection of deposition temperature and solvent can have such a beneficial effect on the blend microstructure. The overall roughness of the blend films has two contributions: i) internal roughness of the predominantly crystalline P(VDF-TrFE) matrix and, more importantly, ii) the roughness originating from the difference in domain height between P(VDF-TrFE) and PFO. Our coating experiments show that it is this latter contribution which shows the strong dependence on deposition temperature. This is supported by the fact that the film roughness of P(VDF-TrFE):PFO blends was not found to change upon annealing, which leads to the crystallization of the ferroelectric.[9]

To understand how the roughness depends on domain height differences we performed time-resolved level-set numerical simulations of cross-sections of phase separating blend layers according to the protocol recently published by Michels et al.[14,17] Topology development during phase separation was allowed by treating the ambient air as a separate fluid phase with a strong incompatibility with the blend components (to avoid "evaporation" of the polymers). In order to do this with our current three-component model, the presence of solvent was discarded. We emphasize that the driving force for de-mixing in these blends predominantly stems from the repulsion between PFO and P(VDF-TrFE) expressed by an (effective) Flory–Huggins interaction parameter $\chi_{PFO\text{-}P(VDF\text{-}TrFE)}$, and not from the interaction with the solvent. This observation is in line with previous conclusions concerning the driving force for de-mixing in solution processed polymer/PCBM blends.[18] In other words, although this simplification will influence the exact layer formation mechanism as a function of time, it does not affect our conclusions concerning the explanation for the temperature-dependence of the roughness induced by PFO domain protrusion.

The development of layer topology, as well as its temperature dependence, can be understood once it is assumed that a substrate and/or air interface-directed effect is playing a role during de-mixing. Despite the lack of evidence for a wetting layer consisting of one the polymers in the final dry blend film,[9] it might be that surface-induced stratification does play a role during the initial stages of de-mixing. At later times, the stratified film may break up in a laterally discrete domain structures, eventually

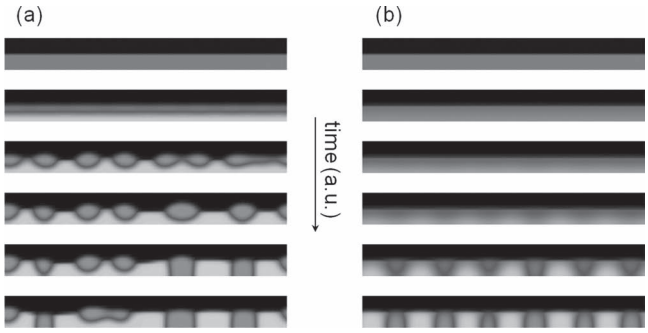

Figure 3. Evolution of blend topography with time. Simulated cross sections of blend films are presented as a function of time (the time increases from top to bottom): a) simulation at low temperature by taking $\chi_{PFO\text{-}P(VDF\text{-}TrFE)} = 0.6$ and b) simulation at high temperature by taking $\chi_{PFO\text{-}P(VDF\text{-}TrFE)} = 0.4$.

leaving no wetting layer in the final blend film. This order of events has been observed previously by others.[19] In the present simulation we enforced a stratification effect by assuming a difference in interaction between the polymer components with the air-interface by defining: $\chi_{PFO\text{-}air} = 0.8$ and $\chi_{P(VDF\text{-}TrFE)\text{-}air} = 0.9$ (effectively representing a difference in surface tension). We note that these values are purely phenomenological and arbitrarily chosen. The only constraints we applied is that these values are in the limit of non-solubility ($\chi > 0.5$) and exceed the polymer-polymer repulsion to avoid "mixing" of the air with the polymeric phases.

The P(VDF-TrFE):PFO blend most likely exhibits upper critical solution temperature behavior.[17] As mentioned above, the repulsive interaction between the polymers, thus, decreases with temperature.[20] In the simulations the temperature dependence of the polymer–polymer interaction was quantitatively expressed by choosing $\chi_{PFO\text{-}P(VDF\text{-}TrFE)} = 0.6$, to represent a low temperature, and $\chi_{PFO\text{-}P(VDF\text{-}TrFE)} = 0.4$, to represent a high temperature. Time snapshots of the simulations are presented by **Figure 3** (panel (a) low temperature, high $\chi_{PFO\text{-}P(VDF\text{-}TrFE)}$; (b) high temperature, low $\chi_{PFO\text{-}P(VDF\text{-}TrFE)}$).

The simulation clearly shows two important aspects: i) the weak repulsion between the polymers at high temperature slows down phase separation, assuming the diffusivity of the components not to depend significantly on temperature and ii) the stratification effect is less pronounced at elevated temperature, leading to a reduction in roughness at any time during de-mixing. The simulations, although representing a simplified version of the physical reality, qualitatively explain the smoothening effect of an increased deposition temperature by a reduction of the polymer–polymer repulsion.

6. Domain Size Development with Blend Composition

The AFM images of wire-bar coated films from cyclohexanone can furthermore be quantitatively analyzed by counting the number of PFO domains and measuring the domain diameter and effective area. The diameter and number of domains are presented in **Figure 4**a,b as a function of composition. A rather narrow size distribution of the PFO domains is found for all blend ratios. Figure 4a shows that the mean lateral size of the domains increases with PFO content up to about 1.5 μm at 50 wt%. The size distribution obtained is comparable to that reported previously for blends of rir-P3HT and P(VDF-TrFE).[9] We note that a square root dependence is expected when the number of domains remains constant. However, Figure 4b shows that the number of domains decreases almost linearly with the reciprocal PFO content, i.e. the phase morphology coarsens with increasing PFO content. This enhanced coarsening is a strong evidence for an increase in the phase separation kinetics. At the moment of vitrification of the blend, the de-mixing process will have proceeded further than in case of a blend with a lower PFO/P(VDF-TrFE) ratio. The increased de-mixing kinetics are explained by the fact that at PFO/P

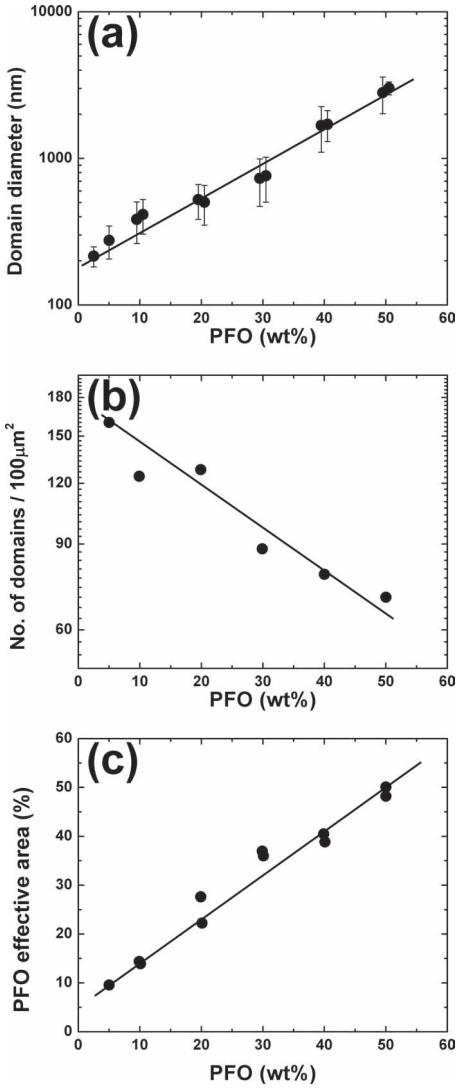

Figure 4. Quantitative analysis of AFM images of the P(VDF-TrFE):PFO blend films wire-bar coated form cyclohexanone at 50 °C. a) domain diameter as a function of PFO content on a semilogaritmic scale. b) the number of domains as a function of PFO content. c) Linear increase in the effective area of PFO domains as a function of PFO content in the film, representing the consistency of the AFM measurement. The solid lines are a guide to the eye.

(VDF-TrFE) ratios closer to unity, one moves away from the spinodal line in the ternary phase diagram, thus increasing the thermodynamic contribution $\left(\left|\frac{\partial^2 F}{\partial \varphi^2}\right|\right)$ to the Onsager coefficient. We note that the effective PFO coverage, calculated from domain density and diameter, increases linearly with PFO content showing that the analysis of the AFM images is internally consistent (Figure 4c).

The relatively narrow size distribution excludes phase separation mechanisms by nucleation and growth and confirms that the microstructure is formed via spinodal decomposition. As stated above, the strongly phase separated microstructure originates from the incompatibility of P(VDF-TrFE) and PFO. Michels et al. for instance predicted that the strong repulsion between PFO and P(VDF-TrFE) causes a negative curvature of the Gibbs free energy of mixing of the blend $\left(\frac{\partial^2 F}{\partial \varphi^2} < 0\right)$ over nearly the entire composition range. This implies a (near) absence of a metastable region in the ternary phase diagram for solvent/PFO/P(VDF-TrFE), practically excluding liquid phase de-mixing via nucleation and growth, and indicating that spinodal decomposition is the dominating de-mixing mechanism, irrespective of blend composition and deposition method.

In addition, (non-equilibrium) temperature/composition phase diagrams (**Figure 5**) obtained from differential scanning calorimetry first heating scans of blend films, cast at room temperature from cyclohexanone reveal a small depression of the melting temperature of P(VDF-TrFE) from 159 °C to 150 °C when adding up to 50 wt% PFO. This is a further indication of the limited compatibility of these two polymers. We note that the latter seems even more pronounced when using THF as solvent, for which our thermal analysis data suggests that the P(VDF-TrFE) films cast from THF feature a simple monotectic phase behavior with a broad miscibility gap of the two components over essentially the entire composition range.

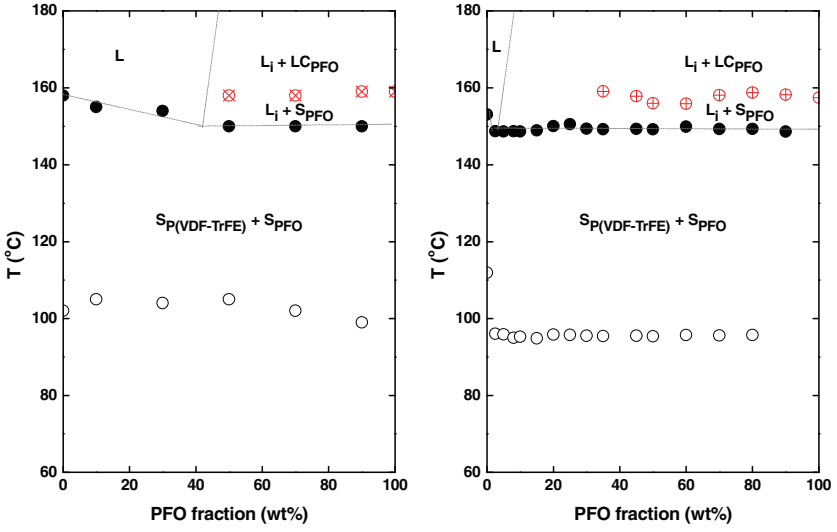

Figure 5. Binary non-equilibrium temperature/composition diagrams of P(VDF-TrFE):PFO blends cast from cyclohexanone (left) or THF (right), followed by solvent evaporation at ambient. The diagrams were constructed with peak transition temperatures recorded during the first heating scan in DSC. Black symbols represent melting of the P(VDF-TrFE), white symbols its Curie transition, and the red circles the transition of PFO into a liquid crystalline phase. L_i, denotes the P(VDF-TrFE) melt, and S_{PFO}, $S_{P(VDF-TrFE)}$ solid phases of PFO and P(VDF-TrFE), respectively.

Interestingly, at the composition where we observe the melting temperature of P(VDF-TrFE) in the non-equilibrium phase diagram of blend films cast from cyclohexanone to remain constant (≥50 wt% PFO), a change in the microstructure compared to the 80:20 blends is observed. At a higher PFO content the microstructure is inverted; spherical P(VDF-TrFE) domains are then embedded in a PFO matrix. At the same time the topographic contrast changes. The AFM height images show that the PFO domains, obtained at low PFO content, protrude from the P(VDF-TrFE) matrix, while P(VDF-TrFE) domains, obtained at high PFO content, are at lower height than the PFO matrix.

The explanation for the protrusion of the PFO domains is two-fold: i) P(VDF-TrFE) has a considerably higher density than PFO (1.8 g cm^{-3} vs. ≈1 g cm^{-3}) and ii) the solvents used in this work (THF and cyclohexanone) are better solvents for P(VDF-TrFE) than for PFO. This difference in solvent compatibility causes the PFO phase to be more concentrated during de-mixing than the P(VDF-TrFE) phase. Upon solidification, the relatively dilute P(VDF-TrFE) will therefore collapse around the PFO domains, which probably have vitrified in an earlier stage. A similar observation has been reported by Steiner et al.[21] on solution-processed films of poly(styrene)/poly(methyl methacrylate) (PS/PMMA) blends. Depending on solvent choice, the topology could be directed from PMMA domain protrusion, via smooth films to PS domain protrusion.

The difference in packing is confirmed by XRD measurements. Grazing incidence XRD diffraction scans of thin films as a function of PFO content are presented in **Figure 6**. From the scans it becomes immediately clear that PFO is predominantly amorphous while P(VDF-TrFE) is semicrystalline. All films show a single diffraction peak at 19.8° 2θ (d = 4.48 Å), corresponding to the (1.1.0)/(2.0.0) peak of the low temperature ferroelectric phase of P(VDF-TrFE). We note that before annealing, an additional broad feature is present at a lower angle, which probably originates from the presence of a phase resembling the paraelectric phase of the PVDF homopolymer. After annealing at 140 °C however, this non-ferroelectric conformation is transferred completely into the ferroelectric phase.

7. Scaling Analysis

The AFM height profiles were also analyzed from the power spectral density (PSD) as a function of spatial frequency, f. The PSD is calculated from 1D line scans as:

$$\mathrm{PSD}(f) = \frac{1}{L}\left|\int_0^L h(x)\exp(i2\pi f x)\mathrm{d}x\right|^2 \qquad (1)$$

where $h(x)$ is the apparent topographical height with respect to the mean height ($\langle h \rangle = 0$) calculated on images with scan length L. The PSD are presented in **Figure 7**a as a function of PFO content. The plateau at low spatial frequency denotes a white spectrum with absence of nonlocal correlations along the

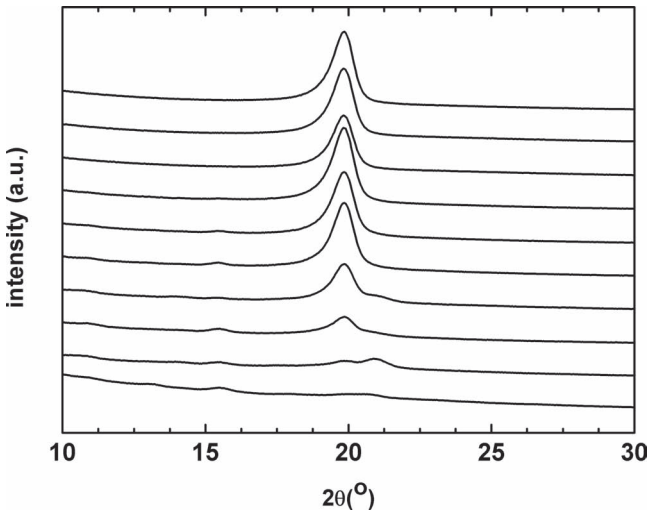

Figure 6. Grazing incidence XRD diffraction scans of thin P(VDF-TrFE):PFO films as a function of PFO content. The films were wire-bar coated form cyclohexanone and annealed for 2 h in vacuum at 140 °C.

scan line. At high frequencies the height fluctuations are spatially correlated. The PSD shows a power law decay as PSD(f) ~ $f^{-\gamma}$ over more than three decades, which is a fingerprint of a self-affine or spatially-correlated surface. A self-affine morphology is obtained for thin films grown under non-equilibrium conditions, here by spin-coating or wire-bar coating. A similar morphology is then preserved upon a change in magnification after rescaling of the height. The self-affinity is further proof for de-mixing to occur via spinodal decomposition, during which the amplitude of a density fluctuation at one preferred wavelength grows at the expense of fluctuations corresponding to different wavelengths. The surface roughness, σ, then follows a power law decay as $\sigma \approx L^{\alpha}$ with the roughness exponent α given by $\alpha = (\gamma - d)/2$ where d is the line scan dimension, here $d = 1$ from Equation (1). From Figure 7a we extract at high spatial frequency a value for α of about 0.5.

The value of α is related to the solidification mechanism; for instance a value of α around unity is typical for a diffusion dominated process. The value derived here of 0.5 suggests that the thin film solidification follows the Kardar-Parisi-Zhang universality class of growth processes.[22] This can occur when the uniformity in solute density is not preserved. Here we start from a homogeneous wet film. Upon solvent evaporation a heterogeneous dry film is formed. Due to the difference in solvent compatibility between the two polymers, as explained in Section 6, the density is not constant over the film, as is reflected by the different heights of the PFO and P(VDF-TrFE) domains. We note however that a definite assignment cannot yet be made; the surface roughness then has to be analyzed as a function of e.g., layer thickness.

The correlation length ξ is the inverse of the breakdown frequency separating the power law decay from the PSD plateau. This correlation length represents the range over which the roughness scales with the probed length. For instance, scaling analysis of thermally induced spinodally decomposed thin films of polycarbonate-polymethylmethacrylate have shown that the correlation length is similar to the domain diameter.[23] A closer look at the PSD spectra of Figure 7a shows that for the present films there are two inflection points. The coherence lengths calculated from both points are presented in Figure 7b as a

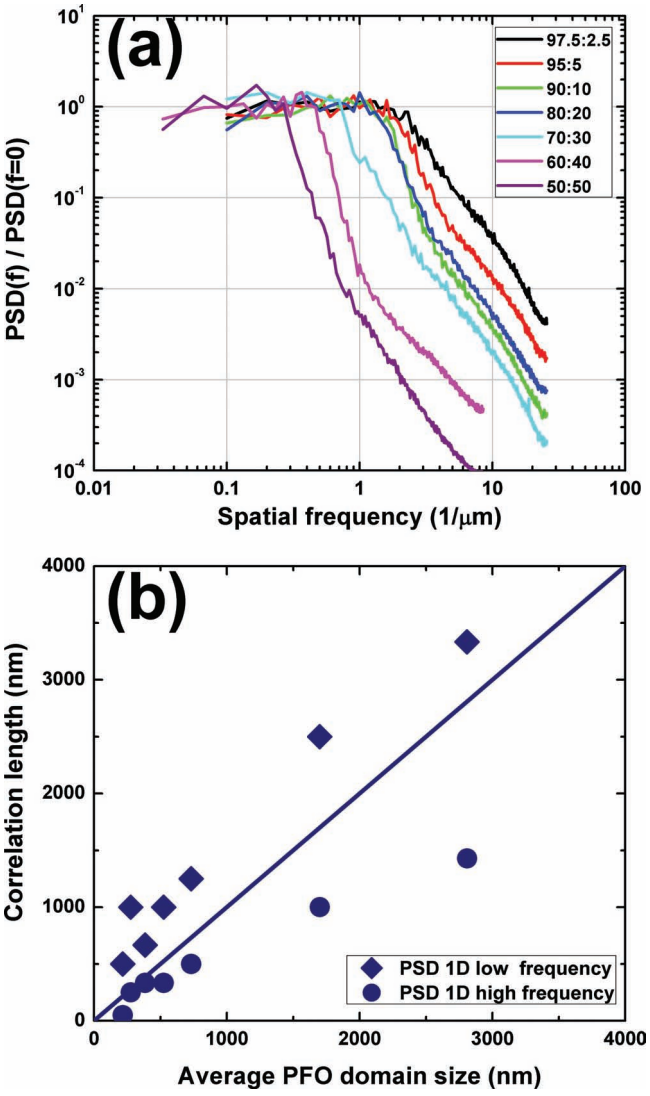

Figure 7. a) 1D PSD as a function of spatial frequency on a double logarithmic scale of P(VDF-TrFE):PFO blend films wire-bar coated from cyclohexanone. PSD was calculated from 10 μm by 10 μm AFM height topography images. The composition is indicated in the legend. The PSD is normalized to the value of the low frequency plateau. b) The correlation lengths calculated from the PSD as a function of average domain diameter determined from the AFM images of Figure 4a. The squares and circles correspond to the low and high frequency inflection points, respectively.

function of the domain diameter as obtained from the AFM images for films with different PFO content. It appears that the correlation lengths scale with the minimum and maximum domain diameter as obtained from the AFM images. The average values show a good agreement with the AFM domain diameter. We note that similar values for the correlation lengths were obtained from the radial, or 2D isotropic, PSD spectra.

8. Rectifying Bistable Diodes

Finally, ferroelectricity and memory functionality were investigated as a function of PFO content using films wire-bar coated at 50 °C, from cyclohexanone. The ferroelectric polarization

and coercive field of neat P(VDF-TrFE) capacitors amounted to 6 μC cm^{-2} and 50 MV m^{-1}, respectively, in good agreement with literature data. The remnant polarization of the blends, measured with a pulse technique, linearly decreases with PFO content; for 10% PFO the polarization amounted to about 90% of that of neat P(VDF-TrFE) capacitors, i. e. 5 μC m^{-2}. Diodes were fabricated using a LiF/Al top electrode and a Au bottom electrode. Both LiF and Au form an injection limited contact on PFO for electrons and holes, respectively. The corresponding barriers for electron and hole injection are 0.6 eV and 1.3 eV.

Current density voltage characteristics for 90:10 blend diodes with film thicknesses of 300 nm and 100 nm are presented in **Figure 8**. We discuss first biases below the coercive voltage of P(VDF-TrFE). In the forward direction holes are injected from gold and electrons from LiF/Al. In the reverse direction there is no current flowing, holes cannot be injected from LiF/Al and electrons cannot be injected form gold. The diodes are rectifying. In forward bias, above the coercive voltage of P(VDF-TrFE), the injection barrier is modulated by the ferroelectric polarization. The diodes switch at the coercive field of the P(VDF-TrFE), corresponding to 14 V and 5 V for the 300 nm and 100 nm thick film respectively. The ferroelectric polarization points toward the Au anode. Both injection barriers effectively can be disregarded and the diodes switch to the on-state. The forward current density is comparable to that reported for rir-P3HT:P(VDF-TrFE) blend diodes.[9] In reverse bias, no current flows. When the reverse bias surpasses the coercive voltage, polarization reversal occurs. The ferroelectric polarization now points toward the LiF/Al cathode. Effectively, both injection barriers then increase and no current is flowing irrespective of the bias. The diode is in the off-state. The final result is a current-voltage characteristic of a bistable rectifying diode with a large current modulation.

The main achievement in Figure 8 is that by reducing the layer thickness a switching voltage well below 10 V is realized. Due to the smooth morphology of the films, the yield of functional diodes is about unity, which indicates that electronic characteristics can be tailored from the outset while processing parameters can be adjusted according to the phase behavior of the active compounds.

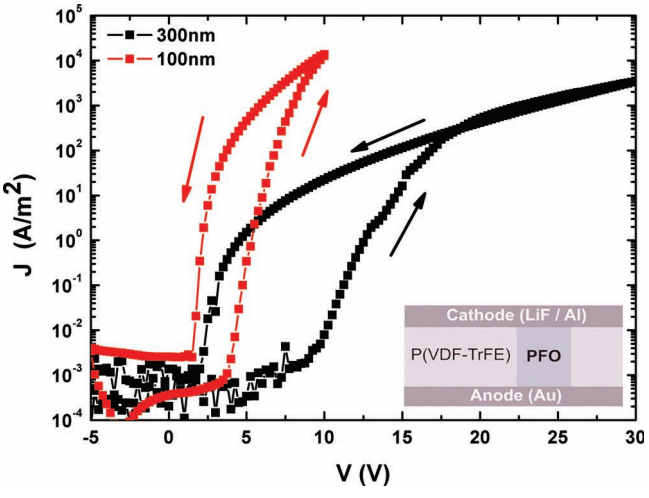

Figure 8. Current density voltage (*J–V*) characteristics of P(VDF-TrFE):PFO (90:10) blend diodes with film thickness of 100 nm (red) and 300 nm (black). Arrows indicate the scan direction. The films were wire-bar coated from cyclohexanone and subsequently annealed for 2 h in vacuum at 140 °C. The inset shows the diode layout.

9. Summary and Conclusion

This work gives a detailed description of our investigative efforts and optimization of the processing of smooth films of phase separated blends of the semiconducting polymer poly(9,9-dioctylfluorenyl-2,7-diyl) and the ferroelectric random copolymer poly(vinylidene fluoride-trifluoroethylene), being the active layer in non-volatile bistable rectifying diodes. Previously reported films of such blends exhibit a high surface roughness. Therefore, thick films are typically applied in order to prevent shorts, yielding high switching voltages and low yield. In contrast, the optimized procedure described in this work allows reduction of the film thickness in diodes as well as in capacitors without the formation of shorts upon evaporation of the top electrode. As a consequence, lower switching voltages can be used.

In order to arrive at a drastically reduced film roughness we have systematically varied blend composition, solvent, and deposition temperature, using wire-bar coating as deposition method as this allows significantly improved control over the deposition temperature compared to spin-coating. At low PFO:P(VDF-TrFE) ratios the dried blend films consist of disk-shaped PFO domains embedded in a P(VDF-TrFE) matrix. The morphology inverts once the P(VDF-TrFE) becomes the minor component. AFM analysis reveals that the film roughness predominantly originates from the height difference between the P(VDF-TrFE) and the PFO domains. Under optimized processing conditions, however, values for the rms roughness as low as <10 nm are routinely obtained.

To understand the influence of process parameters on layer topology and to explain the marked difference in roughness compared to previously reported films, we have measured the phase diagram of the blend and performed time-resolved numerical simulations of cross-sections of phase separating blend layers. The simulations, although representing a simplified version of the physical reality, qualitatively explain the smoothening effect of an increased deposition temperature by reduction of the considerable repulsion between the polymeric components of the blend, which has been suggested to exhibit UCST behavior. The predicted strong repulsion between PFO and P(VDF-TrFE) is confirmed by the monotectic blend behavior, expressed by the binary phase diagram obtained by DSC.

Analysis of AFM images by the power spectral density shows that the surface is self-affine. The size distribution and the increase in domain size with PFO content exclude a de-mixing mechanism by nucleation and growth and show that the phase separation occurs via spinodal decomposition, even for highly asymmetric blend ratios. This is explained by the fact that the pronounced incompatibility between the two polymers yields a large instable region in the ternary phase diagram solvent/PFO/P(VDF-TrFE).

Due to the drastic reduction in film roughness, and thus the possibility to produce smooth, homogenous PFO:P(VDF-TrFE) blend films of a few tens of nanometers thick, bistable rectifying diodes, which switch at about 5 V, can now be realized at a yield of functional devices of nearly 100%. Importantly, wire-bar coating is employed for film fabrication, which is ideally suited to deposited thin films over large area. What's more, wire-bar coating is widely regarded as a model system for industrial coating methods such

as roll- and slot die coating. Hence, the process developed here is a general concept for incompatible blends and is a major leap towards industrialization of high density non-volatile memories.

10. Experimental Section

Materials and Film Preparation: The random copolymer of P(VDF-TrFE) (65–35%) was purchased from Solvey. The semiconductor component poly(9,9-dioctylfluorenyl-2,7-diyl) end-capped with dimethylphenyl groups (PFO), was purchased from American Dye Source. Both materials were utilized as received. The weight-average molecular weight M_w was measured with gel permeation chromatography (GPC) versus polystyrene standards and amounted to 350 and 90 kg mol^{-1} for P(VDF-TrFE) and PFO. Blend solutions were prepared by co-dissolving P(VDF-TrFE) and PFO in distilled THF or cyclohexanone, typically 2 wt%. Thin films were spin-coated, typically at 2000 rpm, or wire-bar coated (K202 control coater, RK Print) on thoroughly cleaned glass substrates. Spin-coating was performed at 25 °C. In order to accurately vary the deposition temperature, wire-bar coating was used. The films were subsequently annealed for 2 h at 140 °C in vacuum to enhance the crystallinity of the P(VDF-TrFE) phase.

Film Characterization: Differential scanning calorimetry (DSC) was conducted under N_2 atmosphere, on as-cast films, at a scan rate of 10 °C min^{-1}, with a Mettler Toledo DSC 822e instrument. The composition/temperature non-equilibrium phase diagram was deduced from those thermal analysis data: Curie-, melting- and liquid-crystalline transitions were deduced from the peak maxima in the respective thermograms.

Film thickness was measured with a DEKTAK surface profilometer. The surface morphology of these blend films was characterized before and after annealing by AFM (Nanoscope Dimension 3100 Bruker).

X-ray diffraction scans were obtained with a Philips X'pert MPD diffractometer, using the line focus of a Cu-anode X-ray tube. For the grazing incidence setup we used a divergence slit of 0.03 ° and a parallel plate collimator in front of the detector. The incidence angle was fixed during the measurement at an angle of 0.23 ° just above the critical angle of total diffraction.

Device Fabrication and Characterization: Diodes were fabricated on thermally oxidized silicon monitor wafers on which 50 nm thick Au bottom electrodes on a 2 nm Ti adhesion layer were photolithographically defined. The blend films were applied and annealed. LiF (1 nm) capped with 70 nm Al was evaporated through a shadow mask and used as top electrode. The device area varied from 0.059 to 1.38 mm^2. The diodes were stored in N_2. The current-voltage measurements were conducted in air with an Agilent 4155C semiconductor parameter analyzer. The bottom contact was grounded. Electric displacement loops versus electric field for neat P(VDF-TrFE) capacitors were measured using a Sawyer-Tower circuit and gave a coercive field of nearly 50 MV m^{-1}. The remnant polarization amounted to 60–70 μC m^{-2} both in good agreement with literature values. The displacement loop measured for the blend capacitors however is distorted. The presence of PFO in the matrix increases the leakage current. The ferroelectric polarization was therefore determined by pulse measurements using a ferroelectric characterization system (Radiant Technology). A pulse of known polarity is applied to set the diode in a known polarization state. Subsequently two pulses of opposite polarity were applied and the responses were recorded. The response of the first pulse contains information about the switching plus the non-switching currents whereas the second pulse gives the non-switching current of the device. Subtracting the two responses gives the net switching current. Remnant polarization was determined by integration of the net switching current in time.

Acknowledgements

The authors acknowledge Jan Harkema for technical assistance, Harry Wondergem for XRD measurements and Paul Smith for fruitful discussions. The authors acknowledge financial support by Zernike Institute for Advanced Materials and the EC Program (FP7/2007-2013) under grant Agreement No. 248092 of the MOMA Project.

Received: November 29, 2011
Published online: April 10, 2012

[1] G. H. Gelinck, H. E. A. Huitema, E. van Veenendaal, E. Cantatore, L. Schrijnemakers, J. B. P. H. van der Putten, T. C. T. Geuns, M. Beenhakkers, J. B. Giesbers, B. Huisman, E. J. Meijer, E. M. Benito, F. J. Touwslager, A. W. Marsman, B. J. E. van Rens, D. M. de Leeuw, *Nat. Mater.* **2004**, *3*, 106.
[2] H. E. A. Huitema, G. H. Gelinck, J. B. P. H. van der Putten, K. E. Kuijk, C. M. Hart, E. Cantatore, P. T. Herwig, A. J. J. M. van Breemen, D. M. de Leeuw, *Nature* **2001**, *414*, 599.
[3] K. Myny, S. Steudel, S. Smout, P. Vicca, F. Furthner, B. van der Putten, A.K. Tripathi, G.H. Gelinck, J. Genoe, W. Dehaene, P. Heremans, *Org. Electron.* **2010**, *11*, 1176.
[4] E. Cantatore, T. C. T. Geuns, G. H. Gelinck, E. van Veenendaal, A. F. a Gruijthuijsen, L. Schrijnemakers, S. Drews, D. M. de Leeuw, *IEEE J. Solid-State Circuits* **2007**, *42*, 84.
[5] S. R. Forrest, *Nature* **2004**, *428*, 911.
[6] G. W. Burr, B. N. Kurdi, J. C. Scott, C. H. Lam, K. Gopalakrishnan, R. S. Shenoy, *IBM J. Res. Dev.* **2008**, *52*, 449.
[7] K. Asadi, D. M. de Leeuw, B. de Boer, P. W. M. Blom, *Nat. Mater.* **2008**, *7*, 547.
[8] K. Asadi, M. Li, N. Stingelin, P. W. M. Blom, D. M. de Leeuw, *Appl. Phys. Lett.* **2010**, *97*, 193308.
[9] K. Asadi, H. J. Wondergem, R. S. Moghaddam, C. R. McNeill, N. Stingelin, B. Noheda, P. W. M. Blom, D. M. de Leeuw, *Adv. Funct. Mater.* **2011**, *21*, 1887.
[10] K. Asadi, T. G. de Boer, P. W. M. Blom, D. M. de Leeuw, *Adv. Funct. Mater.* **2009**, *19*, 3173.
[11] M. Kemerink, K. Asadi, Blom, P. W. M. Blom, D. M. de Leeuw, *Org. Electron.* **2011**, *13*, 147.
[12] K. Asadi, M. Li, P. W. M. Blom, M. Kemerink, D. M. de Leeuw, *Mater. Today* **2011**, *14*, 592.
[13] K. Asadi, P. W. M. Blom, D. M. de Leeuw, *Adv. Mater.* **2011**, *23*, 865.
[14] J. J. Michels, A. J. J. M. van Breemen, K. Usman, G. H. Gelinck, *J. Polym. Sci. Part B: Polym. Phys.* **2011**, *49*, 1255.
[15] Comparison of the images before and after annealing reveals that the circular domains are PFO domains embedded in the P(VDF-TrFE) matrix. Annealing enhances the crystallinity of P(VDF-TrFE) and has only a minor influence on the microstructure of the predominantly amorphous PFO phase. Previously reported SEM images made on blend films of P(VDF-TrFE) with rir-P3HT have shown that the matrix consists of P(VDF-TrFE) needles in agreement with the known needle-like morphology.
[16] C. Murphy, L. Yang, S. Ray, L. Yu, S. Knox, N. Stingelin, *J. Appl. Phys.* **2011**, *110*, 093523
[17] Extensive description of the theoretical background of these simulations is beyond the scope of this publication and will receive more attention in a follow-up to this work.
[18] S. Nilsson, A. Bernasik, A. Budkowski, E Moons, *Macromolecules* **2007**, *40*, 8291.
[19] S. Y. Heriot, R. A. L. Jones, *Nat. Mater.* **2005**, *4*, 782.
[20] *Polymer Handbook, Vol.2*, (Eds: J. Brandrup, E. H. Immergut, E. A. Grulke), John Wiley & Sons, New York **1999**.
[21] S. Walheim, M. Böltau, J. Mlynek, G. Krausch, U. Steiner, *Macromolecules* **1997**, *30*, 1326.
[22] M. Kardar, G. Parisi, Y. Zhang, *Phys. Rev. Lett.* **1986**, *56*, 889.
[23] P. Viville, F. Biscarini, J. L. Bredas, R. Lazzaroni, *J. Phys. Chem. B.* **2001**, *105*, 7499.